Biochemical Pharmacology 85 (2013) 1234–1245

Contents lists available at SciVerse ScienceDirect

Biochemical Pharmacology

journal homepage: www.elsevier.com/locate/biochempharm

Discovery of a new small-molecule inhibitor of p53–MDM2 interaction using a yeast-based approach

Mariana Leão [a], Clara Pereira [a], Alessandra Bisio [b], Yari Ciribilli [b], Ana M. Paiva [c,d], Neuza Machado [c,d], Andreia Palmeira [c,d], Miguel X. Fernandes [e], Emília Sousa [c,d,**], Madalena Pinto [c,d], Alberto Inga [b], Lucília Saraiva [a,*]

[a] *REQUIMTE, Laboratório de Microbiologia, Departamento de Ciências Biológicas, Faculdade de Farmácia, Universidade do Porto, Rua de Jorge Viterbo Ferreira n.° 164, 4050-313 Porto, Portugal*
[b] *CIBIO, Centre for Integrative Biology, Laboratory of Transcriptional Networks, University of Trento, Via delle Regole, 101, 38123 Trento, Italy*
[c] *Centro de Química Medicinal da Universidade do Porto (CEQUIMED-UP), Faculdade de Farmácia, Universidade do Porto, Rua de Jorge Viterbo Ferreira n.° 164, 4050-313 Porto, Portugal*
[d] *Laboratório de Química Orgânica e Farmacêutica, Departamento de Química, Faculdade de Farmácia, Universidade do Porto, Rua de Jorge Viterbo Ferreira n.° 164, 4050-313 Porto, Portugal*
[e] *Centro de Química da Madeira, Universidade da Madeira, Campus da Penteada, 9000-390 Funchal, Portugal*

ARTICLE INFO

Article history:
Received 17 December 2012
Accepted 30 January 2013
Available online 18 February 2013

Keywords:
Xanthone derivatives
Inhibitor of p53–MDM2 interaction
Computational docking
Yeast-based assays
Antitumor activity

ABSTRACT

The virtual screening of a library of xanthone derivatives led us to the identification of potential novel MDM2 ligands. The activity of these compounds as inhibitors of p53–MDM2 interaction was investigated using a yeast phenotypic assay, herein developed for the initial screening. Using this approach, in association with a yeast p53 transactivation assay, the pyranoxanthone (3,4-dihydro-12-hydroxy-2,2-dimethyl-2*H*,6*H*-pyrano[3,2-b]xanthen-6-one) (**1**) was identified as a putative small-molecule inhibitor of p53–MDM2 interaction.

The activity of the pyranoxanthone **1** as inhibitor of p53–MDM2 interaction was further investigated in human tumor cells with wild-type p53 and overexpressed MDM2. Notably, the pyranoxanthone **1** mimicked the activity of known p53 activators, leading to p53 stabilization and activation of p53-dependent transcriptional activity. Additionally, it led to increased protein levels of p21 and Bax, and to caspase-7 cleavage. By computational docking studies, it was predicted that, like nutlin-3a, a known small-molecule inhibitor of p53–MDM2 interaction, pyranoxanthone **1** binds to the p53-binding site of MDM2.

Overall, in this work, a novel small-molecule inhibitor of p53–MDM2 interaction with a xanthone scaffold was identified for the first time. Besides its potential use as molecular probe and possible lead to develop anticancer agents, the pyranoxanthone **1** will pave the way for the structure-based design of a new class of p53–MDM2 inhibitors.

1. Introduction

Despite the huge diversity of genes implicated in tumorigenesis, the p53 tumor suppressor protein stands out as a master regulator of various signaling pathways in this process. The many roles of p53 as a tumor suppressor include the ability to induce cell cycle arrest, DNA repair, senescence, and apoptosis, among others [1–4]. The p53 activity is ubiquitously lost in cancers either by mutation in the *TP53* gene, or by inactivation of its protein, thereby indicating its relevance as a therapeutic target in cancer. About half of all human cancers express a wild-type (wt) p53 form, which is inactivated due to the over-expression of the main endogenous negative regulator, murine double minute 2 (MDM2). The oncoprotein MDM2 binds p53 and negatively regulates p53 activity by direct inhibition of p53 transcriptional activity and enhancement of p53 degradation *via* the ubiquitin–proteasome pathway. Restoration of p53 activity by inhibiting the p53–MDM2 interaction represents an appealing therapeutic strategy for many wt p53 tumors with over-expressed MDM2, and has therefore been the focus of a large effort in drug discovery [1–4].

* Corresponding author. Tel.: +351 220428584; fax: +351 226093390.
** Corresponding author. Tel.: +351 220428689; fax: +351 226093390.
E-mail addresses: esousa@ff.up.pt (E. Sousa), lucilia.saraiva@ff.up.pt (L. Saraiva).

0006-2952/$ – see front matter © 2013 Elsevier Inc. All rights reserved.
http://dx.doi.org/10.1016/j.bcp.2013.01.032

The successful development of inhibitors of protein–protein interactions remains a remarkable challenge for medicinal chemists owing to issues that include general lack of small-molecule scaffolds for drug design, the typical flatness of the interface, the difficulty of distinguishing real from artifactual binding, and the size and character of typical small-molecule libraries [5,6]. In spite of this, an increasing number of small-molecule inhibitors of p53–MDM2 interaction have been developed during the last years. Most of these inhibitors have been obtained using techniques such as computational chemistry, which enables to provide increased specificity and affinity for the target [7]. Although many of these small-molecules have shown potent *in vitro* activity, only a limited number of compounds have demonstrated to possess desirable pharmacokinetic properties and acceptable toxicity profiles in *in vivo* evaluations. To date, the most studied chemotypes have been cis-imidazolines (such as nutlins), benzodiazepines, and spiro-oxindoles. Proofs of concept studies with some of these compounds have demonstrated that inhibitors of p53–MDM2 interaction have therapeutic potential against tumors with a wt p53 form [1–4]. Efforts are in progress to identify new scaffolds of inhibitors of p53–MDM2 interaction with improved biological activities. These molecules are particularly required as molecular probes and have the potential to be developed as anticancer drug candidates [1–4].

Xanthone derivatives have been widely reported as potential anticancer agents [reviewed in [8,9]]. In fact, in the last years, molecular modifications developed by our research group on the tricyclic xanthone scaffold led to potent inhibitors of the growth of several human tumor cell lines [10–14]. Particularly, prenylated xanthone derivatives have drawn attention due to their potency and selectivity against breast adenocarcinoma MCF-7 tumor cells, with wt p53 and overexpressed MDM2 [12]. This was in fact corroborated by a recent work, in which we showed that one of the tested prenylated xanthones exhibited a higher potency against tumor cells with a wt p53 form (MCF-7) than against tumor cells with a mutant p53 form (breast MDA-MB-231) [15]. In addition, reports from other authors have strictly related the antitumor activities of two prenylated xanthones, gambogic acid and α-mangostin, with the activation of a p53-dependent pathway [16–18]. Together, these works raised the hypothesis that xanthone derivatives may represent a promising chemical scaffold to look for new inhibitors of p53–MDM2 interaction.

In the present work, with the virtual screening of a library of xanthone derivatives, potential novel MDM2 ligands were identified, and their activities as inhibitors of p53–MDM2 interaction were investigated using yeast cell-based screening assays. Using this approach, the pyranoxanthone 3,4-dihydro-12-hydroxy-2,2-dimethyl-2*H*,6*H*-pyrano[3,2-b]xanthen-6-one (**1**; Fig. 1), was identified as a promising inhibitor of p53–MDM2 interaction, which successfully activated p53 and downstream cell signaling in human tumor cells. With our findings, a new small-molecule inhibitor of p53–MDM2 interaction with a xanthone scaffold was here identified for the first time.

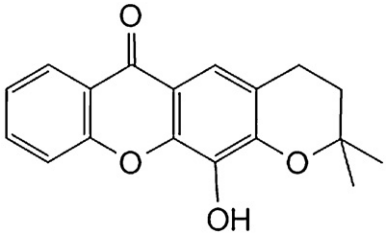

Fig. 1. Chemical structure of 3,4-dihydro-12-hydroxy-2,2-dimethyl-2*H*,6*H*-pyrano[3,2-b]xanthen-6-one (pyranoxanthone **1**).

2. Materials and methods

2.1. Compounds

14 xanthone derivatives were investigated: 3,4-dihydro-12-hydroxy-2,2-dimethyl-2*H*,6*H*-pyrano[3,2-b]xanthen-6-one (**1**), 3,4-bis-(3-methylbut-2-enyloxy)-9*H*-xanthen-9-one (**2**), 3-(3-methylbut-2-enyloxy)-4-hydroxy-9*H*-xanthen-9-one (**3**), (±)-2,3-dihydro-3-(4-hydroxy-3-methoxyphenyl)-2-(hydroxymethyl)-11*H*-1,4-dioxino[2,3-b]xanthen-11-one (**4**), 1-(6-bromohexyloxy)-9*H*-xanthen-9-one (**5**), 3,4-dihydroxy-9*H*-xanthen-9-one (**6**), 3,6-dihydroxy-9*H*-xanthen-9-one (**7**), 1-carbaldehyde-4-hydroxy-3-methoxy-9*H*-xanthen-9-one (**8**), 2,2′,4,4′-tetracetylbenzophenone (**9**), 2-(((*S*)-oxiran-2-yl)methoxy)-1-hydroxy-9*H*-xanthen-9-one (**10**), 1,3-dihydroxy-2-methyl-9*H*-xanthen-9-one (**11**), 2,3-dihydro-10-hydroxy-3,3-dimethyl-11-(2-methylbut-3-en-2-yl)pyrano [2,3-c]xanthen-7(1*H*)-one (**12**), 4-hydroxy-1((isobutylamino)-methyl)-3-methoxy-9*H*-xanthen-9-one (**13**), and 2,3-dihydro-6-hydroxy-3,3,5-trimethylpyrano[2,3-c]xanthen-7(1*H*)-one (**14**). These compounds were obtained and characterized according to described procedures [10–15,19,20]. Nutlin-3a was from Alexis Biochemicals (Grupo Taper, Sintra, Portugal). Doxorubicin was from Sigma–Aldrich (Sintra, Portugal). All tested compounds were dissolved in dimethyl sulfoxide (DMSO; Sigma–Aldrich, Sintra, Portugal).

2.2. Plasmids

For the yeast phenotypic assay, the yeast expression vectors pGADT7-(*LEU2*) encoding human MDM2 (kindly provided by Dr. Xue-Min Zhang from National Center of Biomedical Analysis, China) with *ADH1* constitutive promoter, and pLS89-(*TRP1*) encoding human wt p53 (kindly provided by Dr. Richard Iggo from Swiss Institute for Experimental Cancer Research, Switzerland) with *GAL1-10* inducible promoter were used. For the yeast transactivation assay, the yeast expression vectors pTSG-(*TRP*) encoding human wt p53 under the control of a *GAL1* inducible promoter [21] and pRB24-(*HIS3*) encoding human MDM2 under the control of a *PGK1* constitutive promoter (kindly provided by Dr. Rainer Brachmann from Irvine University, CA, USA), were used.

2.3. Yeast strain, transformation, and growth conditions

For the yeast growth-inhibition assay, *Saccharomyces cerevisiae* CG379 was co-transformed using the standard lithium acetate method. For selection of co-transformed yeasts, cells were routinely grown in a minimal selective medium with 2% (w/w) glucose, 0.7% (w/w) yeast nitrogen base without amino acids from Difco (Quilaban, Sintra, Portugal) and all the amino acids required for yeast growth (50 μg mL^{-1}) except leucine and tryptophan, to approximately 1 optical density at 600 nm (OD_{600}). To induce expression of wt p53 and MDM2, yeasts were diluted to 0.05 OD_{600} into selective induction medium with 2% (w/w) galactose and 2% (w/w) raffinose (instead of glucose), and incubated at 30 °C under continuous orbital shaking (200 r.p.m.) for approximately 42 h (time required by control yeast, co-transformed with the empty vectors pLS239 and pGADT7, to achieve 0.45 OD_{600}). Yeast growth was analyzed by counting the number of colony-forming units (CFU) per mL (CFU mL^{-1}) after 2 days incubation at 30 °C on Sabouraud Dextrose Agar plates from Liofilchem (Frilabo, Porto, Portugal).

2.4. Effects of compounds on yeast cell growth

Co-transformed yeast cells were incubated in selective induction medium in the presence of 10 μM nutlin-3a, 10 μM

xanthones **1–12** or 0.1% DMSO only, for approximately 42 h, at 30 °C, under continuous orbital shaking. Yeast cell growth was analyzed as described in Section 2.3. Results were estimated considering as 100% growth the number of CFU obtained with the control yeast (co-transformed with the empty vectors).

2.5. Yeast cell cycle analysis

Flow cytometric analysis of DNA content was performed using Sytox Green Nucleic Acid, as described [22]. Briefly, 1×10^7 cells were fixed in 70% (v/v) ethanol, incubated with 250 μg mL^{-1} RNase A (Sigma–Aldrich, Sintra, Portugal) and 1 mg mL^{-1} Proteinase K (Sigma–Aldrich, Sintra, Portugal), and further incubated with 10 μM Sytox Green Nucleic Acid from Invitrogen (Alfagene, Carcavelos, Portugal). For the flow cytometric analysis the FACSCalibur flow cytometer from BD Biosciences (Enzifarma, Porto, Portugal) and the CellQuest software from BD Biosciences (Enzifarma, Porto, Portugal) were used. Yeast cell cycle phases were identified and quantified using ModFit LT software (Verity Software House Inc., Topsham, USA).

2.6. Dual-luciferase yeast p53 transactivation assay

Dual-luciferase yeast p53 transactivation assay was performed basically as reported [23]. Briefly, a diploid yeast reporter strain was constructed by mating yLFM-PUMA, RFM-M2 strain with BY4704 strain. For selection of co-transformed yeasts, cells were routinely grown in minimal selective medium with all the amino acids required for yeast growth (50 μg mL^{-1}) except for tryptophan and histidine. To induce expression of human wt p53, yeast cultures were diluted to approximately 0.1 OD_{600} in selective induction medium containing 0.048% (w/w) galactose and 2% (w/w) raffinose. Yeast cells, diluted in selective induction medium as referred above, were seeded into 96-well plates (120 μL/well) and incubated in the presence of 10 μM nutlin-3a, 10 μM xanthones or 0.1% DMSO solvent only, for 16 h (time required by yeast cells to achieve ~0.5 OD_{600}), at 30 °C, under continuous orbital shaking (150 r.p.m.). 10 μL cell cultures was then transferred to a white 384-well plate, followed by 10 μL of 2× Passive Lysis Buffer (Promega, Milan, Italy), and plates were incubated for 15 min at room temperature with continuous orbital shaking (500 r.p.m.). Afterward, 10 μL of *Firefly* Luciferase Bright Glo substrate (Promega, Milan, Italy) were added to the cell suspension and the light units were measured with a luminometer (Mithras LB940 plate reader-Berthold Technologies, Milan, Italy or Infinite M-200, Tecan, Milan, Italy). To measure *Renilla* activity, 5 μL of the *Firefly* Luciferase Substrate (Luciferase Assay Reagent, LARII, Promega, Milan, Italy), followed by the addition of 5 μL of the Stop&Glow buffer (Promega, Milan, Italy), and the light units were measured again with a luminometer. In this assay, since the expression of luciferase occurs in a p53-dependent manner, the p53 transcriptional activity is reflected by the luciferase activity, which was quantified in the presence or absence of the tested compounds.

2.7. Human tumor cell lines and growth conditions

The human breast adenocarcinoma-derived MCF-7 cell line was obtained from the InterLab Cell Line Collection, ICLC (Genoa, Italy). The human colon adenocarcinoma HCT116 cell line harboring a wt p53 form (HCT116 p53$^{+/+}$) and its isogenic derivative, in which p53 has been knocked out (HCT116 p53$^{-/-}$) were kindly provided by Dr. B. Vogelstein (The Johns Hopkins Kimmel Cancer Center, Baltimore, MD, USA). Cell lines were routinely cultured in RPMI with ultraglutamine medium from Lonza (VWR, Carnaxide, Portugal) supplemented with 10% fetal bovine serum from Gibco (Alfagene, Carcavelos, Portugal) and maintained in a humidified incubator at 37 °C with 5% CO_2 in air.

2.8. Dual-luciferase reporter assay in human tumor cell lines

Dual-luciferase reporter assay in human tumor cell lines was performed basically as reported in [24]. Briefly, 5×10^4 cells/well were seeded into 24-well plates and incubated for 24 h before transfection. Cells were transfected at approximately 80% confluence using the Myrus LT-1 reagent (Tema Ricerca, Milan, Italy), and according to the manufacturer's instructions. Specifically, 350 ng of the pG13-luc reporter vector was used along with 50 ng of the control pRLSV40 plasmid introduced to normalize the transfection efficiency. After transfection, cells were treated with 1.5 μM doxorubicin, 10 μM nutlin-3a, 10 μM xanthones or DMSO only, for 16 h. Cells were harvested and the luciferase assay was carried out using the dual-luciferase reagent as described in Section 2.6.

2.9. Western blot analysis

To analyze protein expression in yeast, samples were lysed in Cellytic™ Y Cell Lysis Reagent (Sigma–Aldrich, Sintra, Portugal) in the presence of EDTA-free protease inhibitor cocktail (Sigma–Aldrich, Sintra, Portugal). To analyze protein expression in human tumor cell lines, 1.5×10^5 cells/well were transferred to 6 well-plates, allowed to adhere for 24 h, and then incubated with compounds for 4, 8 and 16 h. Whole cell lysates were then prepared by lysing the cells with RIPA buffer (50 mM Tris–HCl pH 8, 150 mM NaCl, 1% NP-40, 0.5% sodium deoxycholate, 0.1% SDS). Following whole protein quantification using the Bio-Rad Protein Assay (Bio-Rad, Lisboa, Portugal), proteins (20 μg for yeast; 50 μg for human tumor cell lines) were electrophoresed on 12% SDS-PAGE and transferred to an Amersham nitrocellulose membrane from GE Healthcare (VWR, Carnaxide, Portugal). Membranes were blocked with 5% milk and probed with a mouse monoclonal anti-p53 antibody (1:500; DO-1) from Santa Cruz Biotechnology (Frilabo, Porto, Portugal), a mouse monoclonal anti-MDM2 antibody (1:200; Ab-1, OP46) from Calbiochem (VWR, Carnaxide, Portugal), a mouse monoclonal anti-caspase-7 antibody (1:500; B4-G2) from Santa Cruz Biotechnology (Frilabo, Porto, Portugal), which detects the caspase-7 full length precursor and the large subunit (LS) of cleaved caspase-7, or a mouse monoclonal anti-Bax antibody (1:1000; 2D2) from Santa Cruz Biotechnology (Frilabo, Porto, Portugal), followed by an anti-mouse horseradish-peroxidase (HRP)-conjugated secondary antibody (1:5000) from Santa Cruz Biotechnology (Frilabo, Porto, Portugal). For p21 detection, membranes were probed with a rabbit polyclonal anti-p21 antibody (1:2000; C-19) from Santa Cruz Biotechnology (Frilabo, Porto, Portugal), followed by an anti-rabbit horseradish-peroxidase (HRP)-conjugated secondary antibody (1:5000) from Santa Cruz Biotechnology (Frilabo, Porto, Portugal). For loading control, membranes were stripped and reprobed with a mouse monoclonal anti-yeast phosphoglycerate kinase (Pgk1p) antibody (1:5000) from Molecular probes (Alfagene, Carcavelos, Portugal) for yeast, or a rabbit polyclonal anti-actin antibody (1:8000; I19-R) from Santa Cruz Biotechnology (Frilabo, Porto, Portugal) for tumor cell lines. The signal was detected with the ECL Amersham kit from GE Healthcare (VWR, Carnaxide, Portugal) and the Kodak GBX developer and fixer (Sigma–Aldrich, Sintra, Portugal). Band intensities were quantified using the Bio-Profil Bio-1D++ software (Vilber-Lourmat, France).

2.10. Docking of a library of xanthones in MDM2 and p53

To prepare a library of virtual xanthones and known inhibitors of p53–MDM2 interaction, 55 xanthone derivatives [10–15,19,20],

two known inhibitors of the p53–MDM2 interaction [25], and several known non-ligands [26,27] were drawn (ChemSketch, ACD/Labs 2007) and subjected to energy minimization (ArgusLab version 4.0.1 for Windows) by molecular mechanics using the force field method [28].

Docking simulations in MDM2 (pdb code: 1YCR) were undertaken in AutoDock Vina [29]. AutoDock Vina considered the target conformation as a rigid unit, while the ligands were allowed to be flexible and adaptable to the target. A search exhaustiveness of 8 was employed. The 9 lowest energy conformations for each ligand were retrieved. Chimera 1.6.1 [30] and Pymol 0.99 [31] were used for visual inspection of results and graphical representations.

2.11. Statistical analysis

Data were analyzed statistically using the SigmaStat 3.5 software. Differences between means were tested for significance using Student's *t*-test ($P < 0.05$).

3. Results

3.1. Development of a yeast phenotypic assay for the screening of inhibitors of p53–MDM2 interaction

A previous work performed by our group showed that expression of human wt p53 in *S. cerevisiae* induced growth inhibition associated with S-phase cell cycle arrest [22]. Here, it is shown that although the single expression of human MDM2 in yeast did not interfere with the cell growth (therefore represented by the control yeast, transformed with the empty vectors, treated with DMSO only in Figs. 2B and 3A) and cell cycle progression, its co-expression with wt p53 significantly reduced the p53-induced growth inhibition and cell cycle arrest (Fig. 2A–C). These results strengthens the previously reported conservation in yeast of the negative effect of MDM2 on p53 activity [reviewed in [32]], and gave rise to a possible use of these cells in the development of a simple growth-inhibition screening assay to search for inhibitors of p53–MDM2 interaction. In this yeast assay, inhibitors of p53–MDM2 interaction would abolish

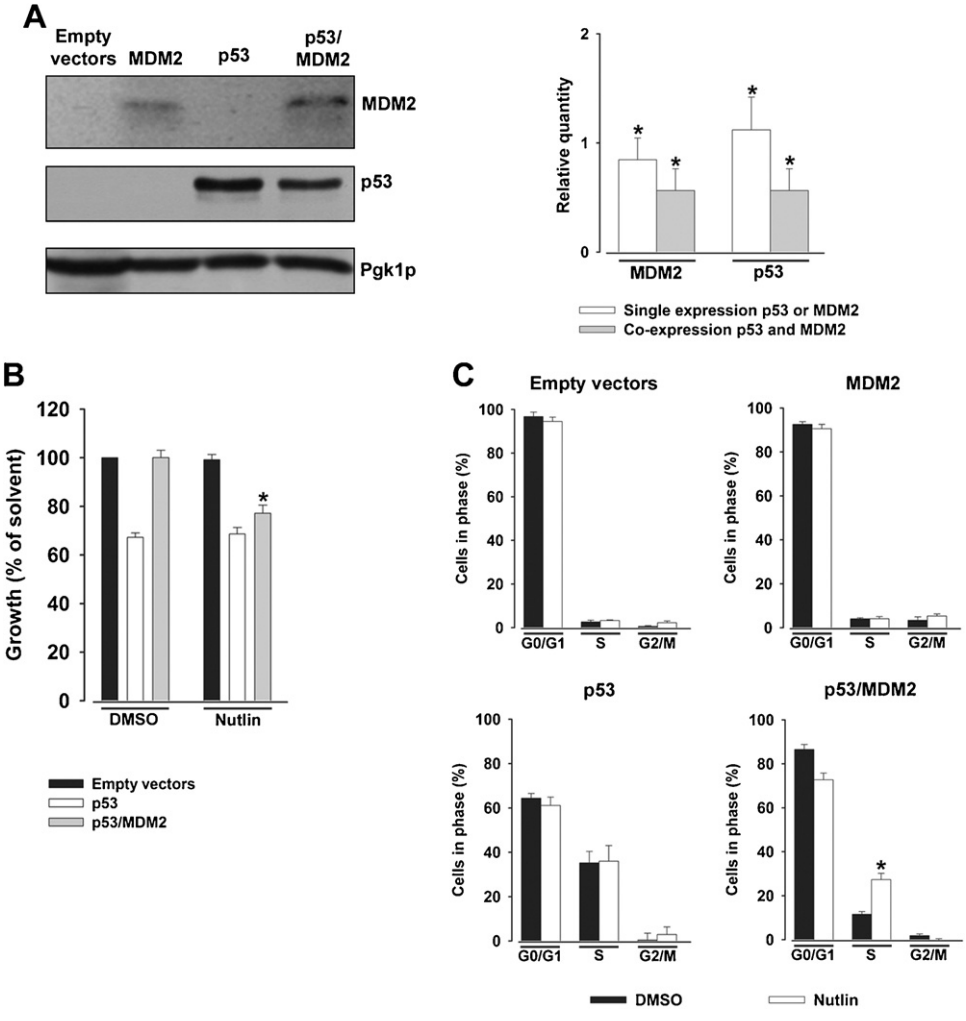

Fig. 2. Nutlin-3a reduces the negative effect of MDM2 on p53 activity in yeast. Co-transformed yeast cells were incubated in selective induction medium in the presence of 10 μM nutlin-3a or DMSO only, for 42 h. (A) Expression of human wt p53 and/or human MDM2 in yeast was confirmed by Western blot analysis. Pgk1p was used as loading control. Immunoblots represent one of two independent experiments. In the quantification of MDM2/p53 band intensities, values are mean ± S.E.M. of two independent experiments; values significantly different from control yeast (empty vectors): $^*P < 0.05$. (B) Effects of nutlin-3a on the growth of control yeast, yeast expressing only p53 and yeast co-expressing p53 and MDM2. Results are plotted setting as 100% growth the number of CFU obtained with control yeast. The growth of yeast expressing MDM2 alone treated with nutlin-3a was approximately 100%, and therefore it is represented by the control yeast treated with DMSO only. Data are mean ± S.E.M. of five independent experiments; values obtained with yeast co-expressing p53 and MDM2 treated with nutlin-3a significantly different from DMSO only ($^*P < 0.05$). (C) Effects of nutlin-3a on the yeast cell cycle progression of control yeast, yeast expressing only MDM2 or p53 and yeast co-expressing p53 and MDM2. Yeast cell cycle phases were quantified by flow cytometry; data are mean ± S.E.M. of two independent experiments; values significantly different from DMSO only ($^*P < 0.05$).

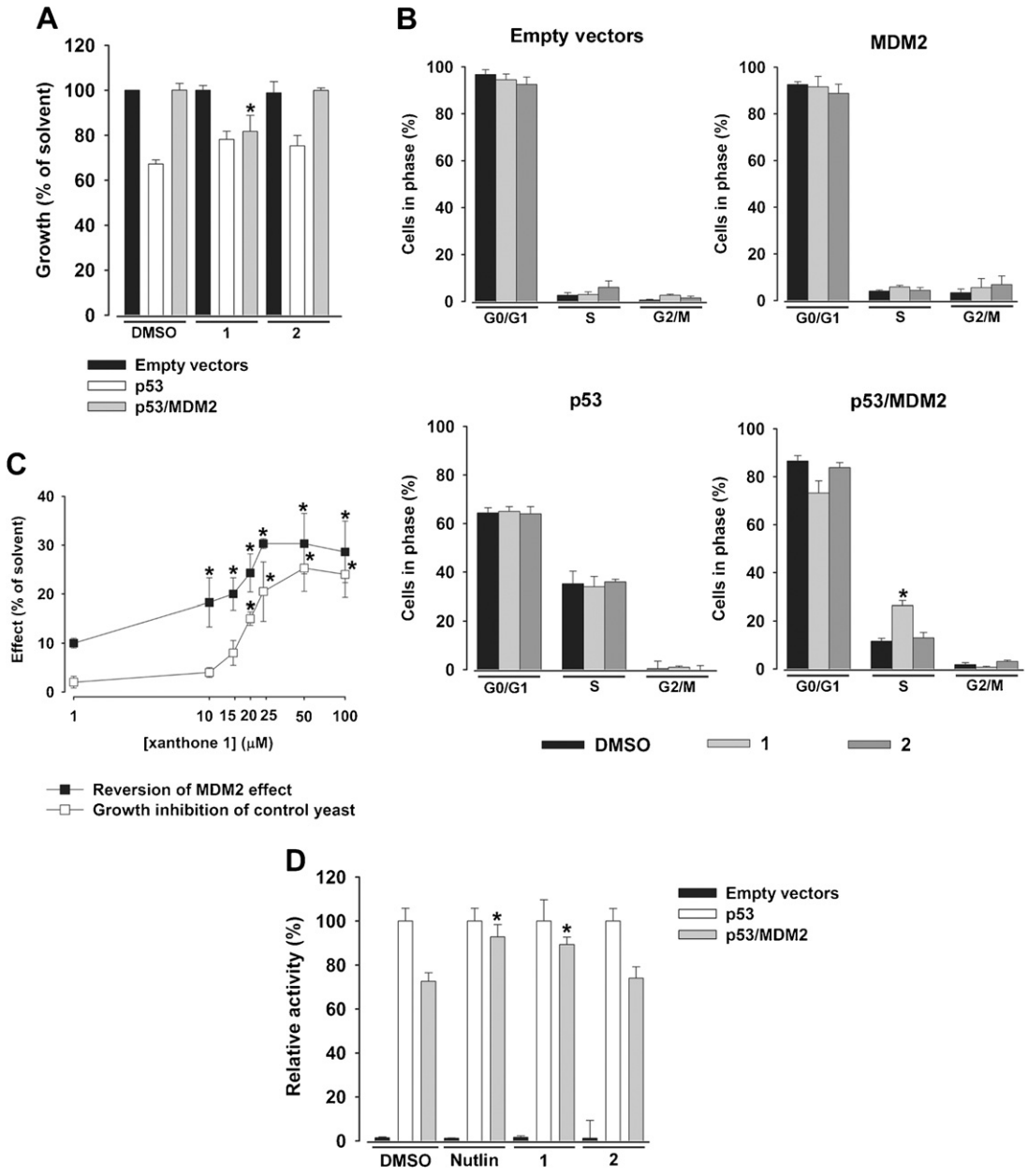

Fig. 3. Pyranoxanthone **1** reduces the negative effect of MDM2 on p53 activity in yeast. Co-transformed yeast cells were incubated in induction selective medium in the presence of 10 μM xanthones **1** and **2** (as representative of non-active xanthones) or DMSO only, for 42 h (in A–C) or 16 h (in D). (A) Effects of xanthones **1** and **2** on the growth of control yeast (empty vectors), yeast expressing only p53 and yeast co-expressing p53 and MDM2. Results are plotted setting as 100% growth the number of CFU obtained with control yeast treated with DMSO only. The growth of yeast expressing MDM2 alone treated with compounds was approximately 100%, and therefore it is represented by the control yeast. Data are mean ± S.E.M. of five independent experiments; values obtained with yeast co-expressing p53 and MDM2 treated with compounds significantly different from DMSO only (*$P < 0.05$). (B) Effects of xanthones **1** and **2** on the yeast cell cycle progression of control yeast, yeast expressing only MDM2 or p53 and yeast co-expressing p53 and MDM2. Yeast cell cycle phases were quantified by flow cytometry; data are mean ± S.E.M. of two independent experiments; values significantly different from DMSO only (*$P < 0.05$). (C) Effects of 1–100 μM xanthone **1** on the reduction of MDM2 negative effect on p53-induced growth inhibition in yeast co-expressing p53 and MDM2 and on the growth inhibition of control yeast. Data are mean ± S.E.M. of four independent experiments; values significantly different from DMSO only (*$P < 0.05$). (D) Effects of xanthones **1** and **2** on the p53-dependent transcriptional activity in control yeast, yeast expressing only p53 and yeast co-expressing p53 and MDM2. Dual-luciferase yeast p53 transactivation assay was performed with the p53 response element PUMA fused to a luciferase gene. Nutlin-3a was used as positive control. Results are plotted as relative to the transcriptional activity achieved by p53 alone (set to 100%). Presented are mean ± S.E.M. of four independent experiments; values obtained with yeast co-expressing p53 and MDM2 treated with compounds significantly different from DMSO only (*$P < 0.05$).

or abate the negative effect of MDM2 on p53, restoring the p53-induced growth inhibition and S-phase cell cycle arrest. The assay was, in fact, validated testing nutlin-3a, the known inhibitor of p53–MDM2 interaction [33,34]. The treatment of yeast cells co-expressing p53 and MDM2 with 10 μM nutlin-3a for 42 h markedly reduced the negative effect of MDM2 on p53-induced growth inhibition and cell cycle arrest, without interfering with the activity of p53 or MDM2 when expressed alone (Fig. 2B and C; in Fig. 2B similar effects of nutlin-3a were obtained on control yeast and yeast cells expressing only MDM2). In fact, in the presence of nutlin-3a approximately 68% and 74.6% of the p53-induced growth inhibition and S-phase cell cycle arrest, respectively, were re-established (Table 1; Fig. 2B and C). Concentrations of nutlin-3a lower than 10 μM did not significantly reduce the negative effect of MDM2 on p53-induced growth inhibition and cell cycle arrest. Moreover, for concentrations of nutlin-3a higher than 10 μM, a cytotoxic effect on control yeast was observed (data not shown).

Table 1
Effects of compounds on the inhibitory activity of MDM2 on p53-induced yeast growth inhibition.

Compounds	Growth inhibition (% of p53 effect)
DMSO	0.2 ± 4.2
Nutlin-3a	67.8 ± 3.3
1	55.8 ± 5.5
2	0.12 ± 1.06
3	20.1 ± 5.6
4	−0.8 ± 9.6
5	7.06 ± 9.1
6	−5.29 ± 1.2
7	−7.71 ± 2.0
8	−5.80 ± 1.5
9	−8.61 ± 2.0
10	*ND*
11	*ND*
12	*ND*

Yeast cells co-expressing p53 and MDM2 were incubated in galactose selective medium in the presence of 10 μM compound or DMSO only, for 42 h. Nutlin-3a was used as positive control. The effect obtained with p53 alone was considered 100% growth inhibition. Data represent mean ± S.E.M. of five independent experiments. *ND*: not determined (a cytotoxic effect on control yeast was observed).

Altogether, with the obtained results a yeast phenotypic assay, based on simple measurements of yeast cell growth and analysis of yeast cell cycle, was developed that could enable us to search for inhibitors of p53–MDM2 interaction.

3.2. Virtual screening of a library of xanthone derivatives to search for potential MDM2 ligands

The virtual screening of a library of xanthone derivatives resulted in a list of potential MDM2 ligands ranked according to their binding affinities. Docking simulations in PyRx/AutoDock Vina produced nine docked conformations for each ligand. The total number of compounds screened was 60. These small-molecules correspond mainly to xanthone derivatives with diverse substituents such as simple oxygenated, prenylated, lignoids, and others [10–15,19,20]. Two known inhibitors of p53–MDM2 interaction, nutlin-3a, and (4-chlorophenyl)[3-(4-chlorophenyl)-7-iodo-2,5-dioxo-1,2,3,5-tetrahydro-4*H*-1,4-benzodiazepin-4-yl]acetic acid (bzd), were used in the docking studies as positive controls along with known non-ligands of MDM2, used as negative controls.

MDM2 residues Gly58, Asp68, Val75, and Cys77 are critical for the interaction with p53 [35]. In the virtual screening against MDM2 (PDB code: 1YCR), to study only the interactions established by a ligand in this binding site, the grid box was placed in a position so that the ligand could not interact elsewhere with the MDM2 (Fig. A1). The binding affinity values found for the best scoring conformations of the well-characterized inhibitors of p53–MDM2 interaction, which are known to establish interactions with MDM2 protein, were between −6.9 (bzd) and −5.6 (nutlin-3a) kcal mol^{-1}. A total of 46 xanthone derivatives showed binding affinity values in this range (Table A1), with the pyranoxanthone **1** (Fig. 1) revealing the highest binding affinity (−7.6 kcal mol^{-1}). However, limiting the docking studies to the above mentioned grid, the nutlin-3a showed a binding affinity lower than the expected [36]. Nutlin-3a was previously predicted to contact with nine MDM2 amino acids [36] and, by limiting the interaction site using the grid box, nutlin-3a was not allowed to contact with all the MDM2 amino acids. Subsequently, the study of the interactions established by the ligands with the entire MDM2 protein (1YCR) was performed removing the grid box. In this case the absolute binding affinity value of nutlin-3a rose to −7.4 kcal mol^{-1} binding at a different site in the MDM2 protein (Table A2). However, the binding affinity of the hit pyranoxanthone **1** was the same (−7.6 kcal mol^{-1}). A possible explanation for these results is that there are no other interaction sites other than the 4 amino acids selected with the grid box in the MDM2 protein that would lead to higher pyranoxanthone **1** binding affinity.

Based on the overall *in silico* results and on the IC_{50} (concentration required to cause 50% growth inhibition) values against human tumor cells with wt p53 [10,11,13,15,19], the xanthone derivatives **1–14** were selected for the yeast cell-based screening assay (Table 1; xanthones **13** and **14** were not tested due to the low solubility in DMSO).

3.3. Identification of pyranoxanthone *1* as a promising inhibitor of p53–MDM2 interaction using the yeast approach

Using the developed yeast phenotypic assay, the activity of the most promising xanthone derivatives **1–12** on p53–MDM2 interaction was investigated. Since xanthones **10–12** were cytotoxic in control yeast, their effects on p53–MDM2 interaction were not evaluated. Among the tested xanthones, only the pyranoxanthone **1** significantly reduced the MDM2 inhibitory effect on p53 activity (Table 1; Fig. 3A and B; effects of xanthones **2–9** are represented by xanthone **2**), without interfering with the activity of p53 or MDM2 when expressed alone (Fig. 3A and B; in Fig. 3A similar effects of pyranoxanthone **1** were obtained on control yeast and yeast expressing only MDM2). In fact, likewise nutlin-3a, when yeast cells co-expressing p53 and MDM2 were treated with 10 μM of pyranoxanthone **1** for 42 h, approximately 56% and 87% of the p53-induced growth inhibition and S-phase cell cycle arrest, respectively, were re-established (Table 1; Fig. 3A and B). Dose–response curves for the effects of 1–100 μM pyranoxanthone **1** on the reduction of the MDM2 negative effect on p53-induced growth inhibition in yeast co-expressing p53 and MDM2 and on the inhibition of growth of control yeast were obtained (Fig. 3C). The concentration of 10 μM pyranoxanthone **1** was selected as the lower concentration for which a significant reduction of the negative effect of MDM2 on p53-induced growth inhibition was obtained without cytotoxic effects on control yeast. In opposition, xanthones **2–9** did not interfere with the negative effect of MDM2 on p53-induced yeast growth inhibition (Table 1; Fig. 3A; represented by xanthone **2**) and cell cycle arrest (Fig. 3B; represented by xanthone **2**).

The effect of the xanthone derivatives on the negative regulation of p53-dependent transcriptional activity by MDM2 was also analyzed in yeast using a dual-luciferase p53 transactivation assay previously reported in [23]. This assay was carried out in yeast cells co-expressing p53 and MDM2, and used the p53 response element derived from the *BBC3/PUMA* gene fused to a luciferase reporter. The results showed that, likewise to 10 μM nutlin-3a, 10 μM pyranoxanthone **1** significantly increased the luciferase activity. This indicated a reversion of the MDM2 inhibitory effect on p53 transcriptional activity by pyranoxanthone **1** (Fig. 3D). As obtained in the yeast phenotypic assay, xanthones **2–9** did not interfere with the p53 transcriptional activity (Fig. 3D; represented by xanthone **2**).

Altogether, the results obtained in yeast strongly supported that the pyranoxanthone **1** was a promising inhibitor of p53–MDM2 interaction.

3.4. Pyranoxanthone *1* reactivates the p53 activity and downstream cell signaling in human tumor cells

The molecular mechanism of action of pyranoxanthone **1** as inhibitor of p53–MDM2 interaction was further ascertained in human tumor cells harboring wt p53 and overexpressed MDM2, and was compared to that obtained with known small-molecule activators of p53 activity, 1.5 μM doxorubicin and 10 μM nutlin-3a.

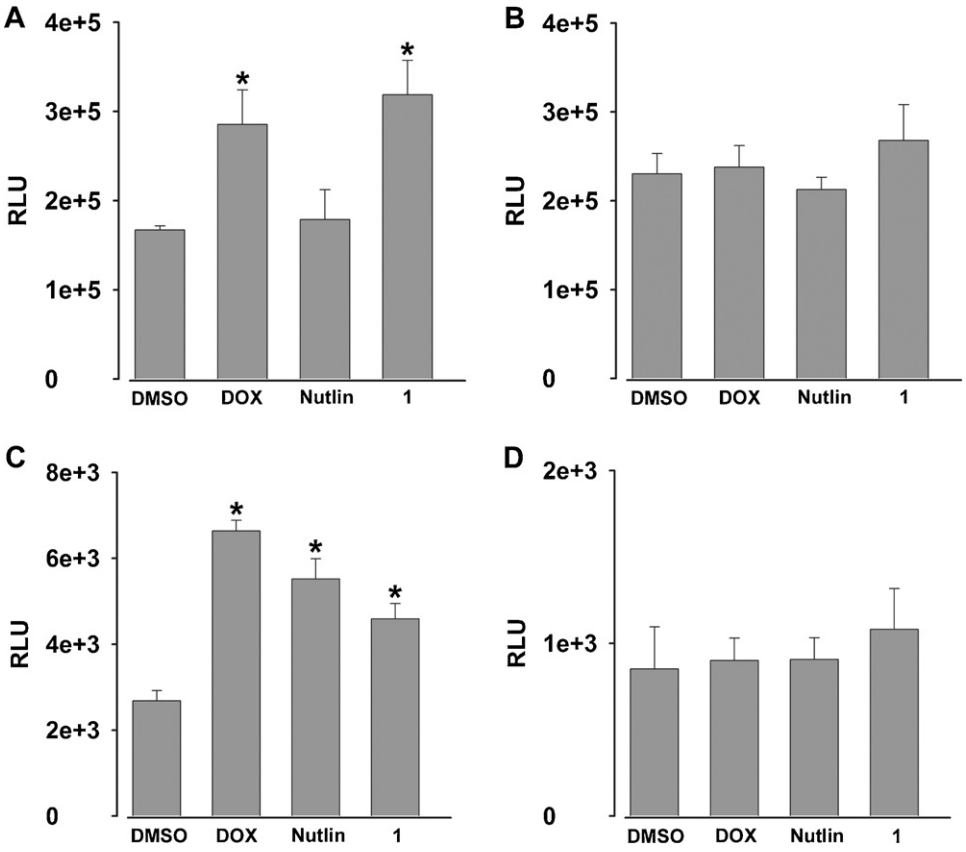

Fig. 4. Pyranoxanthone **1** increases the p53-dependent transcriptional activity in human tumor cells. For the dual-luciferase gene reporter assay, the human tumor cells transfected with the pG13-luciferase reporter vector (or the empty reporter vector) were incubated in the presence of 1.5 μM doxorubicin (DOX), 10 μM nutlin-3a, 10 μM pyranoxanthone **1** or DMSO only for 16 h. Doxorubicin and nutlin-3a were used as positive controls. (A–C) Effects of pyranoxanthone **1** on the pG13-luciferase reporter activity in: (A) HCT116 $p53^{+/+}$, (B) HCT116 $p53^{-/-}$ (negative control of A), and (C) MCF-7 cells. In (D), MCF-7 cells were transfected with the empty reporter vector (negative control of C). RLU, relative light units. Data are mean ± S.E.M. of three independent experiments; values significantly different from DMSO only: $^{*}P < 0.05$.

In order to analyze the effect of pyranoxanthone **1** on p53-dependent transcriptional activity, a p53 reporter assay was performed in human tumor cells with wt p53, HCT116 $p53^{+/+}$ (Fig. 4A) and MCF-7 (Fig. 4C). In parallel, the activity of pyranoxanthone **1** was evaluated in p53 null HCT116 cells (HCT116 $p53^{-/-}$; Fig. 4B) and MCF-7 cells transfected with an empty reporter vector, which served as negative controls (Fig. 4D). In this assay, the synthetic p53 response element pG13 fused to the luciferase reporter gene was used. The obtained results showed that, likewise doxorubicin (in HCT116 $p53^{+/+}$), and doxorubicin and nutlin-3a (in MCF-7), 10 μM pyranoxanthone **1** markedly increased the luciferase activity in HCT116 $p53^{+/+}$ (Fig. 4A) and MCF-7 (Fig. 4C) tumor cells. On the contrary, it did not interfere with the luciferase activity in p53-negative control cell lines exposed to the same conditions (Fig. 4B and D). These results demonstrated that the pyranoxanthone **1** successfully activated the p53-dependent transcriptional activity in human tumor cell lines.

The effect of pyranoxanthone **1** on the stabilization of p53 protein levels was also analyzed in HCT116 tumor cells. As expected, similarly to positive controls, 10 μM pyranoxanthone **1** increased the p53 baseline levels upon 4, 8 and 16 h treatments in HCT116 $p53^{+/+}$ cells, suggesting an inhibition of the p53 degradation by MDM2 in these cells (Fig. 5A). However, contrarily to nutlin-3a, for the different tested time points, no increase on MDM2 protein levels was observed in these tumor cells after treatment with 10 μM pyranoxanthone **1** (Fig. 5B). In spite of this, likewise positive controls, 10 μM pyranoxanthone **1** increased the expression levels of other proteins encoded by p53 target genes, namely p21 (Fig. 5C) and Bax (Fig. 5D) after 16 and 8 h treatments, respectively, in HCT116 $p53^{+/+}$ but not in HCT116 $p53^{-/-}$ tumor cells. Similarly, it enhanced the procaspase-7 cleavage to the active caspase-7 (LS) form at the 8 h treatment in HCT116 $p53^{+/+}$ but not in HCT116 $p53^{-/-}$ tumor cells (Fig. 5E).

Altogether, these results confirmed the effectiveness of the pyranoxanthone **1** in human tumor cells with wt p53. In fact, the pyranoxanthone **1** activated the p53-dependent transcriptional activity, and increased the protein levels of p53, p21, Bax and cleaved caspase-7.

*3.5. Analysis of the predicted binding model of pyranoxanthone **1** to MDM2 supports that pyranoxanthone **1** binds to MDM2*

Based on the obtained results, a careful visual inspection of the pyranoxanthone **1** on the limited interaction site of MDM2 was performed by computational docking. As shown in Fig. 6A, the best fitting molecule (pyranoxanthone **1**) adopted a pose within the p53-binding site, filling the space supposedly occupied by the p53 helix. Fig. 6B highlights the polar interaction established between pyranoxanthone **1** and MDM2. In contrast, nutlin-3a–MDM2 interaction revealed no hydrogen bonding (Fig. 6C). This obtained result is in accordance to [36], in which was verified that nutlin-3a binds to MDM2 mainly by hydrophobic interactions, where it is predicted to contact nine MDM2 amino acids, but all without hydrogen bonds.

4. Discussion

To search for new inhibitors of p53–MDM2 interaction several assays have been developed in the last years. However, most of them are actually quite expensive when applied to the screening of

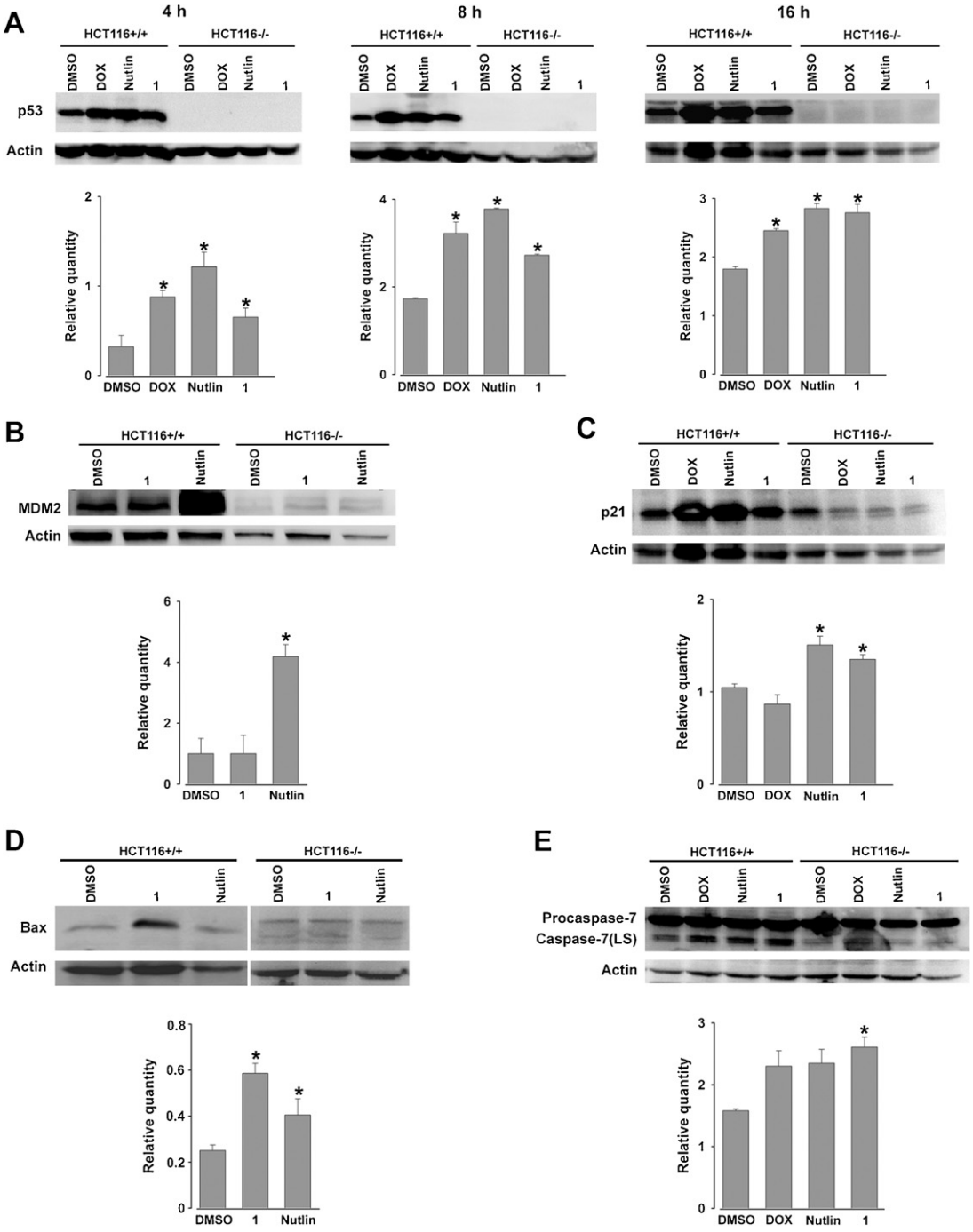

Fig. 5. Pyranoxanthone **1** leads to p53 stabilization, increases p21 and Bax levels, and enhances procaspase-7 cleavage to active caspase-7 in HCT116 p53$^{+/+}$ cells. HCT116 tumor cells were incubated in the presence of 1.5 μM doxorubicin (DOX), 10 μM nutlin-3a, 10 μM pyranoxanthone **1** or DMSO only for 4, 8 and 16 h. Doxorubicin and nutlin-3a were used as positive controls. Protein expression levels were analyzed by Western blot and normalized to the actin loading control. Effects of pyranoxanthone **1** on the protein levels of: (A) p53 at 4, 8 and 16 h; (B) MDM2 at 8 h; (C) p21 at 16 h; (D) Bax at 8 h. (E) Pyranoxanthone **1** enhances procaspase-7 cleavage to the active caspase-7 (LS) form at 8 h. In the quantification of band intensities obtained in A–E, values are mean ± S.E.M. of two independent experiments; values significantly different from DMSO only: $^{*}P < 0.05$.

large libraries of compounds, limiting their use in drug discovery. In the present work, a simple, selective, and reliable yeast growth-inhibition assay was developed to search for novel inhibitors of p53–MDM2 interaction. This assay can be easily adapted to the high-throughput screening of large chemical libraries based on simple measurements of the yeast cell growth in a cost-effective manner [reviewed in [32]]. In this study, the use of this yeast assay led us to the identification of a potential lead compound (pyranoxanthone **1**), thus providing a proof of concept for its effectiveness in the discovery of new inhibitors of p53–MDM2 interaction. The yeast growth-inhibition assay proves to be greatly useful in the initial screening for a first selection of most promising compounds to be tested in more complex cell models.

In this work, using the virtual screening based on multiple binding modes, a set of putative MDM2 ligands with a xanthone scaffold was identified. Based on the generated ranking docking scores, 14 of the potential ligands, exhibiting in our previous studies antiproliferative activity against tumor cells with wt p53 [11,13,15], were selected. The activity of these 14 compounds as inhibitors of p53–MDM2 interaction was subsequently investigated using the

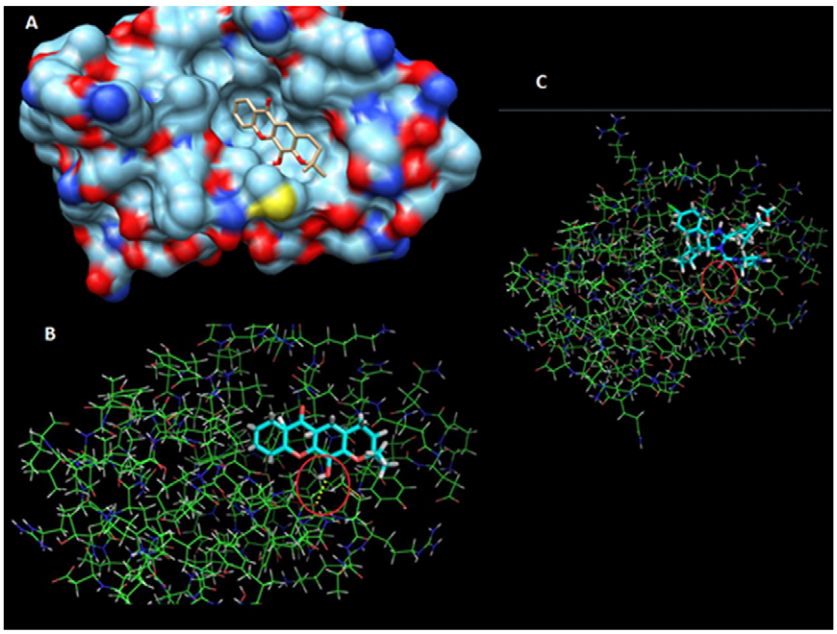

Fig. 6. Predicted binding model using computational docking for the hit pyranoxanthone **1**. (A) Pyranoxanthone **1** in the binding site of MDM2. (B) Polar interaction (highlighted with the red circle) established by pyranoxanthone **1** (blue) in the MDM2 (green) binding site. (C) Absence of hydrogen bond between MDM2 and nutlin-3a. (For interpretation of the references to color in this figure legend, the reader is referred to the web version of the article.)

developed yeast phenotypic screening assay followed by a yeast p53 transactivation assay [described in [23]]. Using this yeast assay, the pyranoxanthone **1** (3,4-dihydro-12-hydroxy-2,2-dimethyl-2*H*,6*H*-pyrano[3,2-b]xanthen-6-one) was identified as a promising inhibitor of p53–MDM2 interaction. Interestingly, the active hit identified in yeast also exhibited the highest binding affinity (-7.6 kcal mol^{-1}) to the MDM2 local of interaction with p53 in the virtual screening. Nevertheless, a correlation between docking scores and activity was not observed and future studies would require considering not only the ligands, but also the target as flexible to improve the accuracy of the docking results.

To further ascertain whether the pyranoxanthone **1** had effects on tumor cells consistent with an inhibition of p53–MDM2 interaction, the activity of this compound was analyzed in human tumor-derived cell lines with wt p53 and overexpressed MDM2. In a recent work, pyranoxanthone **1** revealed a higher potency against tumor cells with wt p53 (MCF-7; $GI_{50} = 5.3 \pm 0.7$) than against tumor cells with mutant p53 (MDA-MB-231; $GI_{50} = 29.0 \pm 3.6$) [15]. Supporting previous results from our group [11,13,15], this work confirmed the effectiveness of pyranoxanthone **1** in tumor cells with wt p53. Most importantly, herein it is shown that, in conformity to what obtained in yeast, the pyranoxanthone **1** mimicked the activity of known small-molecule activators of p53 activity in human tumor cells, leading to the successful activation of p53 and downstream cell signaling.

By computational docking studies it was possible to ascertain that similarly to nutlin-3a, pyranoxanthone **1** binds to MDM2, and therefore activating p53 through inhibition of MDM2 function in tumor cells. However, distinct types of interactions were detected for these two compounds. While interaction of pyranoxanthone **1** with MDM2 involves hydrogen interaction with Gly58, a residue critical for the interaction of MDM2 with p53, nutlin-3a-MDM2 interaction mainly involves hydrophobic interactions.

As a whole, in this work, pyranoxanthone **1** (3,4-dihydro-12-hydroxy-2,2-dimethyl-2*H*,6*H*-pyrano[3,2-b]xanthen-6-one) was identified as a new inhibitor of p53–MDM2 interaction. Our finding thus adds, for the first time, the xanthone scaffold to the list of chemotypes of small-molecule inhibitors of p53–MDM2 interaction. In contrast to nutlin-3a, the pyranoxanthone **1** represents a very promising achiral compound with feasible synthesis and herein different binding modes with MDM2 were predicted. Besides its potential use as molecular probe and possible anticancer agent, pyranoxanthone **1** mainly represents a useful lead compound for the structure-based design of more potent drug-like analogs.

Acknowledgments

This work was supported by FCT (Fundação para a Ciência e a Tecnologia) through REQUIMTE (PEst-C/EQB/LA0006/2011), CEQUIMED-UP (Pest-OE/SAU/UI4040/2011), and the projects FCOMP-01-0124-FEDER-015752 and FCOMP-01-0124-FEDER-011057 also funded by FEDER through the COMPETE program, and by U. Porto/Santander Totta, and in part by the Italian Association for Cancer Research, AIRC (IG #9086). M. Leão (SFRH/BD/64184/2009) and A. Paiva (PTDC/SAU-FCT/100930/2008) and Liga Portuguesa Contra o Cancro/Pfizer are recipients of FCT fellowships. Compounds **9** and **12** were obtained by Dr. Elisangela Costa, compound **14** by Dr. Raquel Castanheiro, and Western blot from Fig. 2A by Dr. Isabel Coutinho to whom we thank.

Appendix A

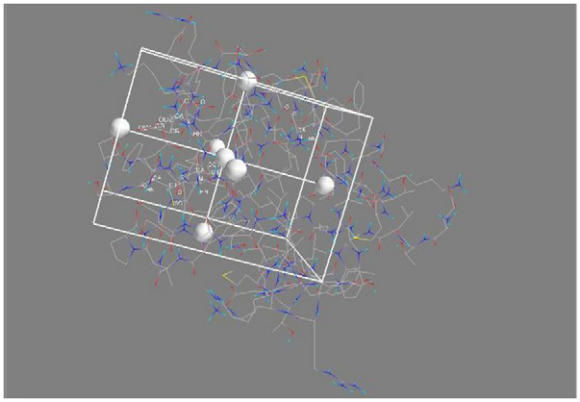

Fig. A1. Grid dimensions and position in the MDM2 in PyRxAutodockVina.

Table A1
Results of docking simulations for MDM2 (with grid box) performed in PyRx/AutoDockVina.

Ligand	Binding affinity (kcal mol^{-1})
3,4-Dihydro-12-hydroxy-2,2-dimethyl-2*H*,6*H*-pyrano[3,2-b]xanthen-6-one (**1**)	−7.6
2,3-Dihydro-10-hydroxy-3,3-dimethyl-11-(2-methylbut-3-en-2-yl)pyrano[2,3-c]xanthen-7(1*H*)-one (**12**)	−7.3
5-Hydroxy-2,2-dimethylpyrano[3,2-b]xanthen-6(2*H*)-one	−7.3
6-Hydroxy-3,3,5-trimethylpyrano[2,3-c]xanthen-7(3*H*)-one	−7.2
6-Hydroxy-3,3-dimethylpyrano[2,3-c]xanthen-7(3*H*)-one	−7.1
3,4-Dihydro-5-hydroxy-2,2-dimethylpyrano[3,2-b]xanthen-6(2*H*)-one	−7.0
2,3-Dihydro-4-hydroxy-2,3,3-trimethylfuro[3,2-b]xanthen-5-one	−7.0
2,3-Dihydro-6-hydroxy-3,3-dimethylpyrano[2,3-c]xanthen-7(1*H*)-one	−6.9
(4-Chlorophenyl)[3-(4-chlorophenyl)-7-iodo-2,5-dioxo-1,2,3,5-tetrahydro-4*H*-1,4-benzodiazepin-4-yl]acetic acid (bzd)[a]	−6.9
3-(3-Methylbut-2-enyloxy)-9*H*-xanthen-9-one	−6.8
3-(3-Methylbut-2-enyloxy)-1-hydroxy-9*H*-xanthen-9-one	−6.7
2,3-Dihydro-6-hydroxy-3,3,5-trimethylpyrano[2,3-c]xanthen-7(1*H*)-one (**14**)	−6.7
(4-(*tert*-Pentyloxy)-2-hydroxyphenyl)(3,4-dihydro-5-hydroxy-2,2-dimethyl-2*H*-chromen-6-yl)methanone	−6.6
3,4-*bis*(3-Methylbut-2-enyloxy)-9*H*-xanthen-9-one (**2**)	−6.6
3-(3-Methylbut-2-enyloxy)-4-hydroxy-9*H*-xanthen-9-one (**3**)	−6.5
3,4-Dihydro-5-hydroxy-2,2-dimethyl-12-(3-methylbut-2-enyl)pyrano[3,2-b]xanthen-6(2*H*)-one	−6.4
2,3-Dihydro-3-(4-hydroxy-3-methoxyphenyl)-2-(hydroxymethyl)-[1,4]dioxino[2,3-a]xanthen-12-one	−6.1
4-Hydroxy-3-methoxy-9*H*-xanthen-9-one	−6.1
2-(((*S*)-Oxiran-2-yl)methoxy)-1-hydroxy-9*H*-xanthen-9-one (**10**)	−6.0
9-Oxo-9*H*-xanthene-3,6-diyl disulfate	−6.0
1,2-Dihydro-5-hydroxy-1,1,2,4-tetramethylfuro[2,3-c]xanthen-6-one	−6.1
3-(3-Methylbut-2-enyloxy)-1-hydroxy-2-methyl-9*H*-xanthen-9-one	−6.1
4-Hydroxy-1-(isobutylamino)-3-methoxy-9*H*-xanthen-9-one (**13**)	−6.0
2,3-Dimethoxy-9*H*-xanthen-9-one	−5.9
3,4-Dihydroxy-9*H*-xanthen-9-one (**6**)	−5.9
4-Hydroxy-9*H*-xanthen-9-one	−5.9
1,7-Dihydroxy-9*H*-xanthen-9-one	−5.9
1,3-Dihydroxy-2-methyl-9*H*-xanthen-9-one (**11**)	−5.9
5,8,10-Trihydroxy-7*H*-benzo[c]xanthen-7-one	−5.9
3-(3-Methylbut-2-enyloxy)-1-hydroxy-4-(3-methylbut-2-enyl)-9*H*-xanthen-9-one	−5.9
1-(6-Bromohexyloxy)-9*H*-xanthen-9-one (**5**)	−5.9
2-Methoxy-9*H*-xanthen-9-one	−5.8
3-Methoxy-9*H*-xanthen-9-one	−5.8
(±)-2,3-Dihydro-3-(4-hydroxy-3-methoxyphenyl)-2-(hydroxymethyl)-11*H*-1,4-dioxino[2,3-b]xanthen-11-one (**4**)	−5.8
1-Hydroxy-9*H*-xanthen-9-one	−5.8
3-(6-Bromohexyloxy)-4-hydroxy-9*H*-xanthen-9-one	−5.8
3,5-Dimethoxy-9*H*-xanthen-9-one	−5.7
4-Methoxy-9*H*-xanthen-9-one	−5.7
3-Hydroxy-9*H*-xanthen-9-one	−5.7
9*H*-xanthen-9-one	−5.7
1-Carbaldehyde-4-hydroxy-3-methoxy-9*H*-xanthen-9-one (**8**)	−5.6
3,4-*bis*(6-Bromohexyloxy)-9*H*-xanthen-9-one	−5.6
1-Methoxy-9*H*-xanthen-9-one	−5.6
2,3-Dihydroxy-9*H*-xanthen-9-one	−5.6
2-Hydroxy-9*H*-xanthen-9-one	−5.6
1,3-Dihydroxy-9*H*-xanthen-9-one	−5.6
3-(3-Methylbut-2-enyloxy)-1-hydroxy-2-methyl-4-(3-methylbut-2-enyl)-9*H*-xanthen-9-one	−5.6
nutlin-3a[a]	−5.6
2,2′,4,4′-Tetracetylbenzophenone (**9**)	−5.5
3,6-Dihydroxy-9*H*-xanthen-9-one (**7**)	−5.5
3-Hydroxy-5-methoxy-9*H*-xanthen-9-one	−5.5
1,2-Dihydroxy-9*H*-xanthen-9-one	−5.5
3,4-Dimethoxy-9*H*-xanthen-9-one	−5.4
3-Hydroxy-4-methoxy-9*H*-xanthen-9-one	−5.4
1,2-Dimethoxy-9*H*-xanthen-9-one	−5.4
(±)-2,3-Dihydro-3-(4-hydroxy-3-methoxyphenyl)-2-(hydroxymethyl)-[1,4]dioxino[2,3-c]xanthen-7-one	−5.3
2-Glucopyranose-9-oxo-9*H*-xanthene-1,3,6,7-tetrayl tetraacetate	−4.3
varacin[b]	−4.2

[a] Positive controls.
[b] Negative control.

Table A2
Results of docking simulations for MDM2 (total protein) done in PyRx/AutoDockVina.

Ligand	Binding affinity (kcal mol^{-1})
3-(3-Methylbut-2-enyloxy)-1-hydroxy-4-(3-methylbut-2-enyl)-9*H*-xanthen-9-one	−8.0
(±)-2,3-Dihydro-3-(4-hydroxy-3-methoxyphenyl)-2-(hydroxymethyl)-11*H*-1,4-dioxino[2,3-b]xanthen-11-one (**4**)	−7.9
3-(3-Methylbut-2-enyloxy)-1-hydroxy-2-methyl-4-(3-methylbut-2-enyl)-9*H*-xanthen-9-one	−7.9
3,4-Dihydro-5-hydroxy-2,2-dimethyl-12-(3-methylbut-2-enyl)pyrano[3,2-b]xanthen-6(2*H*)-one	−7.9
(4-(*tert*-Pentyloxy)-2-hydroxyphenyl)(3,4-dihydro-5-hydroxy-2,2-dimethyl-2*H*-chromen-6-yl)methanone	−7.8
(±)-2,3-Dihydro-3-(4-hydroxy-3-methoxyphenyl)-2-(hydroxymethyl)-[1,4]dioxino[2,3-c]xanthen-7-one	−7.7
3,4-Dihydro-12-hydroxy-2,2-dimethyl-2H,6*H*-pyrano[3,2-b]xanthen-6-one (**1**)	−7.6
3,4-*bis*(3-Methylbut-2-enyloxy)-9*H*-xanthen-9-one (**3**)	−7.6
2,3-Dihydro-10-hydroxy-3,3-dimethyl-11-(2-methylbut-3-en-2-yl)pyrano[2,3-c]xanthen-7(1*H*)-one (**12**)	−7.6
5-Hydroxy-2,2-dimethylpyrano[3,2-b]xanthen-6(2*H*)-one	−7.5
nutlin-3a[a]	−7.4
1,2-Dihydro-5-hydroxy-1,1,2,4-tetramethylfuro[2,3-c]xanthen-6-one	−7.4
6-Hydroxy-3,3,5-trimethylpyrano[2,3-c]xanthen-7(3*H*)-one	−7.4
3,4-Dihydro-5-hydroxy-2,2-dimethylpyrano[3,2-b]xanthen-6(2*H*)-one	−7.3
2,3-Dihydro-6-hydroxy-3,3-dimethylpyrano[2,3-c]xanthen-7(1*H*)-one	−7.3
6-Hydroxy-3,3-dimethylpyrano[2,3-c]xanthen-7(3*H*)-one	−7.3
2,3-Dihydro-3-(4-hydroxy-3-methoxyphenyl)-2-(hydroxymethyl)-[1,4]dioxino[2,3-a]xanthen-12-one	−7.2
2,3-Dihydro-6-hydroxy-3,3,5-trimethylpyrano[2,3-c]xanthen-7(1*H*)-one (**14**)	−7.2
3-(3-Methylbut-2-enyloxy)-9*H*-xanthen-9-one	−7.1
2,3-Dihydro-4-hydroxy-2,3,3-trimethylfuro[3,2-b]xanthen-5-one	−7.1
3-(3-Methylbut-2-enyloxy)-4-hydroxy-9*H*-xanthen-9-one (**2**)	−7.0
3-(3-Methylbut-2-enyloxy)-1-hydroxy-9*H*-xanthen-9-one	−7.0
2,2′,4,4′-Tetracetylbenzophenone (**9**)	−6.9
(4-Chlorophenyl)[3-(4-chlorophenyl)-7-iodo-2,5-dioxo-1,2,3,5-tetrahydro-4*H*-1,4-benzodiazepin-4-yl]acetic acid (bzd)[a]	−6.9
3-(3-Methylbut-2-enyloxy)-1-hydroxy-2-methyl-9*H*-xanthen-9-one	−6.9
5,8,10-Trihydroxy-7*H*-benzo[c]xanthen-7-one	−6.8
9-Oxo-9*H*-xanthene-3,6-diyl disulfate	−6.6
4-Hydroxy-1-(isobutylamino)-3-methoxy-9*H*-xanthen-9-one (**13**)	−6.6
1-(6-Bromohexyloxy)-9*H*-xanthen-9-one (**5**)	−6.5
4-Hydroxy-3-methoxy-9*H*-xanthen-9-one	−6.2
2-(((S)-Oxiran-2-yl)methoxy)-1-hydroxy-9*H*-xanthen-9-one (**10**)	−6.3
3-(6-Bromohexyloxy)-4-hydroxy-9*H*-xanthen-9-one	−6.2
4-Methoxy-9*H*-xanthen-9-one	−6.1
2-Glucopyranose-9-oxo-9*H*-xanthene-1,3,6,7-tetrayl tetraacetate	−6.1
3,4-*bis*(6-Bromohexyloxy)-9*H*-xanthen-9-one	−6.1
2,3-Dimethoxy-9*H*-xanthen-9-one	−6.0
3,4-Dihydroxy-9*H*-xanthen-9-one (**6**)	−6.0
3,5-Dimethoxy-9*H*-xanthen-9-one	−6.0
3-Hydroxy-4-methoxy-9*H*-xanthen-9-one	−6.0
1,3-Dihydroxy-2-methyl-9*H*-xanthen-9-one (**11**)	−6.0
1-Formyl-4-hydroxy-3-methoxy-9*H*-xanthen-9-one (**8**)	−5.9
1,7-Dihydroxy-9*H*-xanthen-9-one	−5.9
1-Methoxy-9*H*-xanthen-9-one	−5.9
2-Methoxy-9*H*-xanthen-9-one	−5.9
3,4-Dimethoxy-9*H*-xanthen-9-one	−5.9
3-Methoxy-9*H*-xanthen-9-one	−5.9
4-Hydroxy-9*H*-xanthen-9-one	−5.9
1-Hydroxy-9*H*-xanthen-9-one	−5.9
1,2-Dihydroxy-9*H*-xanthen-9-one	−5.8
2-Hydroxy-9*H*-xanthen-9-one	−5.8
3-Hydroxy-5-methoxy-9*H*-xanthen-9-one	−5.8
3-Hydroxy-9*H*-xanthen-9-one	−5.8
1,3-Dihydroxy-9*H*-xanthen-9-one	−5.8
1,2-Dimethoxy-9*H*-xanthen-9-one	−5.7
2,3-Dihydroxy-9*H*-xanthen-9-one	−5.7
3,6-Dihydroxy-9*H*-xanthen-9-one (**7**)	−5.7
9*H*-Xanthen-9-one	−5.7
Varacin[b]	−4.5

[a] Positive controls.
[b] Negative control.

References

[1] Lauria A, Tutone M, Ippolito M, Pantano L, Almerico AM. Molecular modeling approaches in the discovery of new drugs for anti-cancer therapy: the investigation of p53–MDM2 interaction and its inhibition by small molecules. Curr Med Chem 2010;17:3142–54.
[2] Wang W, Hu Y. Small molecule agents targeting the p53–MDM2 pathway for cancer therapy. Med Res Rev 2011;32:37.
[3] Kamal A, Mohammed AA, Shaik TB. p53–MDM2 inhibitors: patent review (2009–2010). Expert Opin Ther Pat 2012;22:95–105.
[4] Wang S, Zhao Y, Bernard D, Aguilar A, Kumar S. Targeting the MDM2-p53 protein–protein interaction for new cancer therapeutics. Top Med Chem 2012;8:57–80.
[5] Murray JK, Gellman SH. Targeting protein–protein interactions: lessons from p53/MDM2. Biopolymers 2007;88:657–86.
[6] Wells JA, McClendon CL. Reaching for high-hanging fruit in drug discovery at protein–protein interfaces. Nature 2007;450:1001–9.
[7] Lu SY, Jiang YJ, Zou JW, Wu TX. Molecular modeling and molecular dynamics simulation studies on pyrrolopyrimidine-based alpha-helix mimetic as dual inhibitors of MDM2 and MDMX. J Mol Graph Model 2011;30:167–78.
[8] Pinto MM, Sousa ME, Nascimento MS. Xanthone derivatives: new insights in biological activities. Curr Med Chem 2005;12:2517–38.
[9] Pouli N, Marakos P. Fused xanthone derivatives as antiproliferative agents. Anti-Cancer Agent Me 2009;9:77–98.
[10] Pedro M, Cerqueira F, Sousa ME, Nascimento MSJ, Pinto M. Xanthones as inhibitors of growth of human cancer cell lines and their effects on the proliferation of human lymphocytes in vitro. Bioorg Med Chem 2002;10:3725–30.

[11] Sousa EP, Silva AMS, Pinto MMM, Pedro MM, Cerqueira FAM, Nascimento MSJ. Isomeric kielcorins and dihydroxyxanthones: synthesis, structure elucidation, and inhibitory activities of growth of human cancer cell lines and on the proliferation of human lymphocytes in vitro. Helv Chim Acta 2002;85: 2862–76.
[12] Castanheiro RA, Pinto MM, Silva AM, Cravo SM, Gales L, Damas AM, et al. Dihydroxyxanthones prenylated derivatives: synthesis, structure elucidation, and growth inhibitory activity on human tumor cell lines with improvement of selectivity for MCF-7. Bioorg Med Chem 2007;15:6080–8.
[13] Sousa E, Paiva A, Nazareth N, Gales L, Damas AM, Nascimento MSJ, et al. Bromoalkoxyxanthones as promising antitumor agents: synthesis, crystal structure and effect on human tumor cell lines. Eur J Med Chem 2009;44:3830–5.
[14] Palmeira A, Vasconcelos MH, Paiva A, Fernandes MX, Pinto M, Sousa E. Dual inhibitors of P-glycoprotein and tumor cell growth: (Re)discovering thioxanthones. Biochem Pharmacol 2011;83:11.
[15] Paiva AM, Sousa ME, Camoes A, Nascimento MSJ, Pinto MMM. Prenylated xanthones: antiproliferative effects and enhancement of the growth inhibitory action of 4-hydroxytamoxifen in estrogen receptor-positive breast cancer cell line. Med Chem Res 2012;21:552–8.
[16] Gu HY, Wang XT, Rao SY, Wang J, Zhao J, Ren FL, et al. Gambogic acid mediates apoptosis as a p53 inducer through down-regulation of mdm2 in wild-type p53-expressing cancer cells. Mol Cancer Ther 2008;7:3298–305.
[17] Rong JJ, Hu R, Qi Q, Gu HY, Zhao Q, Wang J, et al. Gambogic acid down-regulates MDM2 oncogene and induces p21(Waf1/CIP1) expression independent of p53. Cancer Lett 2009;284:102–12.
[18] Aisha AF, Abu-Salah KM, Ismail Z, Majid A. In vitro and in vivo anti-colon cancer effects of *Garcinia mangostana* xanthones extract. BMC Complement Altern Med 2012;12:104.
[19] Costa E, Sousa E, Nazareth N, Nascimento MSJ, Pinto MMM. Synthesis of xanthones and benzophenones as inhibitors of tumor cell growth. Lett Drug Des Discov 2010;7:487–93.
[20] Palmeira A, Paiva A, Sousa E, Seca H, Almeida GM, Lima RT, et al. Insights into the in vitro antitumor mechanism of action of a new pyranoxanthone. Chem Biol Drug Des 2010;76:43–58.
[21] Inga A, Storici F, Darden TA, Resnick MA. Differential transactivation by the p53 transcription factor is highly dependent on p53 level and promoter target sequence. Mol Cell Biol 2002;22:11.
[22] Coutinho I, Pereira G, Leao M, Goncalves J, Corte-Real M, Saraiva L. Differential regulation of p53 function by protein kinase C isoforms revealed by a yeast cell system. FEBS Lett 2009;583:3582–8.
[23] Andreotti V, Ciribilli Y, Monti P, Bisio A, Lion M, Jordan J, et al. p53 transactivation and the impact of mutations, cofactors and small molecules using a simplified yeast-based screening system. PLoS One 2011;6:e20643.
[24] Bisio A, Nasti S, Jordan JJ, Gargiulo S, Pastorino L, Provenzani A, et al. Functional analysis of CDKN2A/p16INK4a 5′-UTR variants predisposing to melanoma. Hum Mol Genet 2010;19:1479–91.
[25] Vassilev LT. MDM2 inhibitors for cancer therapy. Trends Mol Med 2007;13: 23–31.
[26] Clement JA, Kitagaki J, Yang Y, Saucedo CJ, O'Keefe BR, Weissman AM, et al. Discovery of new pyridoacridine alkaloids from *Lissoclinum cf. badium* that inhibit the ubiquitin ligase activity of Hdm2 and stabilize p53. Bioorg Med Chem 2008;16:10022–28.
[27] Datta S, Bucks ME, Koley D, Lim PX, Savinov SN. Functional profiling of p53-binding sites in Hdm2 and Hdmx using a genetic selection system. Bioorg Med Chem 2010;18:6099–108.
[28] Kini RM, Evans HJ. Molecular modeling of proteins—a strategy for energy minimization by molecular mechanics in the amber force-field. J Biomol Struct Dyn 1991;9:475–88.
[29] Trott O, Olson AJ. Software news and update AutoDock Vina: improving the speed and accuracy of docking with a new scoring function, efficient optimization, and multithreading. J Comput Chem 2010;31:455–61.
[30] Pettersen EF, Goddard TD, Huang CC, Couch GS, Greenblatt DM, Meng EC, et al. UCSF chimera—a visualization system for exploratory research and analysis. J Comput Chem 2004;25:1605–12.
[31] Seeliger D, de Groot BL. Ligand docking and binding site analysis with PyMOL and Autodock/Vina. J Comput Aided Mol Des 2010;24:417–22.
[32] Pereira C, Leao M, Soares J, Bessa C, Saraiva L. New therapeutic strategies for cancer and neurodegeneration emerging from yeast cell-based systems. Curr Pharm Des 2012;18:4223–35.
[33] Tovar C, Rosinski J, Filipovic Z, Higgins B, Kolinsky K, Hilton H, et al. Small-molecule MDM2 antagonists reveal aberrant p53 signaling in cancer: implications for therapy. Proc Natl Acad Sci U S A 2006;103:1888–93.
[34] Vassilev LT, Vu BT, Graves B, Carvajal D, Podlaski F, Filipovic Z, et al. In vivo activation of the p53 pathway by small-molecule antagonists of MDM2. Science 2004;303:844–8.
[35] Freedman DA, Epstein CB, Roth JC, Levine AJ. A genetic approach to mapping the p53 binding site in the MDM2 protein. Mol Med 1997;3:248–59.
[36] Warner WA, Sanchez R, Dawoodian A, Li E, Momand J. Identification of FDA-approved drugs that computationally bind to MDM2. Chem Biol Drug Des 2012;80:631–7.